Journal of Materials Chemistry B

RSC Publishing

PAPER

View Article Online
View Journal | View Issue

Tuning core–shell SiO_2@CdTe@SiO_2 fluorescent nanoparticles for cell labeling†

Cite this: *J. Mater. Chem. B*, 2013, **1**, 2315

Yian Zhu,[a] Zhen Li,*[b] Min Chen,[c] Helen M. Cooper[c] and Zhi Ping Xu*[a]

Received 12th February 2013
Accepted 8th March 2013

DOI: 10.1039/c3tb20202j

www.rsc.org/MaterialsB

Highly fluorescent SiO_2@CdTe@SiO_2 (SQS) nanoparticles as a new nanoprobe in biomedical imaging have been successfully synthesized by a novel approach. The size of SQS can be tuned from 39 to 76 nm by controlling reaction parameters, including the amount and the type of silica precursor, the ratio of silica precursor to ammonia solution, and the ratio of H_2O to surfactant. The photo- and chemical stability, cytotoxicity and cell uptake of these nanoparticles were investigated. The results demonstrate that these properties are strong size-dependent, and reveal that the minimal shell thickness for effective protection of the embedded CdTe quantum dots is 6 nm. Our findings highlight the importance of controlling particle size and shell thickness during the preparation of fluorescent silica-QDs core–shell nanoparticles, and their potential in cell labeling and imaging.

Introduction

As a potential biolabel, semiconductor quantum dots (QDs) have attracted more and more attention in the last two decades.[1–4] Compared to organic dyes, QDs exhibit excellent optical merits including wide absorption and narrow symmetric emission spectra, size and composition-dependent emission, high fluorescence efficiency, large effective Stokes shift, long fluorescence lifetime, and high resistance to photobleaching and chemical degradation.[5] These merits highlight their superiority in multiplex and long-term fluorescence imaging. However, the practical bioapplications of QDs have to overcome their potential toxicity and instability in the biological environment, in addition to maintaining their bright fluorescence.[6–9] Many efforts have been made to improve QDs' water-solubility, biocompability, photo- and chemical stability, in which modification of QDs with water-soluble and biocompatible organic and/or inorganic shell is a common choice. For example, surface ligand-exchange is often used to make hydrophobic QDs hydrophilic.[10,11] Unfortunately, ligand-exchange can lead to a huge loss in fluorescence due to the change in their surface-properties. Besides ligand-exchange, a number of organic polymers, which are used as drug-carriers, have also been confirmed as suitable coatings for QDs, such as polyethylene glycol (PEG),[12–14] polyethylenimine (PEI),[15,16] and liposomes.[17–19] However, the surface-coated flexible polymers are less resistant to oxygen and chemicals, and have little impact on the improvement of photo- and chemical stability of QDs. Therefore, polymer-modified QDs still face issues of toxicity, instability and the loss of fluorescence, despite the significant progress in recent years.

Compared with organic ligand-modified QDs, QDs coated with an inorganic shell such as silica show higher stability and tunable size. Silica is one of the most popular inert materials for surface modification. Coating QDs with nontoxic silica has a few distinct advantages. (1) Non-porous silica shell can protect QDs from environmental damage and improve their stability. (2) The silica shell can effectively inhibit the release of toxic Cd^{2+} ions and thus reduce QDs' toxicity.[20,21] (3) Silica coating can provide a hydrophilic surface. (4) The silica shell can provide more options for conjugating with biomolecules, since its surface is easily modified with functional groups such as carboxyl, amine, and thiol groups.[22,23] The silica shell can be formed on the surface of QDs by the Stöber method[24–26] or reverse microemulsion approach.[27–29] The Stöber method often yields large nanoparticles (NPs) with a thicker silica shell, while the reverse microemulsion route can produce sub-100 nm NPs.

During modification and functionalization of QDs, the overall particle size has to be strictly controlled because increasing evidence demonstrates that particle size is one of the most important factors that influence their behavior in biological applications, such as cell internalization,[30,31] tumor targeting and penetration,[32,33] *in vivo* systemic and lymphatic biodistribution,[34] and metabolism and clearance.[35] For example, studies of spherical gold NPs, silica NPs, single-walled carbon nanotubes, and QDs have shown that a 50 nm diameter

[a]*ARC Centre of Excellence for Functional Nanomaterials, Australian Institute for Bioengineering and Nanotechnology, The University of Queensland, Queensland 4072, Australia. E-mail: gordonxu@uq.edu.au; Fax: +61-7-33463973*

[b]*Institute for Superconducting & Electronic Materials, The University of Wollongong, NSW 2500, Australia. E-mail: zhenl@uow.edu.au; Fax: +61-2-42215731; Tel: +61-2-42215163*

[c]*The Queensland Brain Institute, The University of Queensland, Queensland 4072, Australia*

† Electronic supplementary information (ESI) available. See DOI: 10.1039/c3tb20202j

is the optimal size in achieving the maximum cellular uptake by some mammalian cells.[36–38] *In vivo* distribution showed that NPs smaller than 6 nm can be excreted by the kidneys and thus are eliminated rapidly, whereas NPs with diameters larger than 200 nm accumulate in the spleen and liver, where they are processed by the mononuclear phagocyte system cells.[35] It should be noted that NPs with a size of 20–60 nm have attracted more interests due to their distinct biodistribution, tumor penetration, and cellular trafficking properties.[39–41] Although the particle size of pure silica NPs produced in water-in-oil reverse microemulsion systems can be effectively tuned by controlling silica precursor amount,[42] surfactant type and concentration,[43] water phase concentration, and ammonia concentration,[44] it is still a challenge to prepare highly fluorescent QDs@silica NPs since the fluorescence of as-synthesized QDs is easily quenched during the coating process. There are a few studies on the preparation of fluorescent QDs@SiO_2 NPs with tunable size.[28,42,45] However, these conventional QDs@SiO_2 NPs have low fluorescence QY and their highest value is <50%, which is much lower than that of original QDs (QY is up to 80%).[45] Their low QY could be due to the difficulty in controlling QD amount in each silica NP because of electrostatic interactions between silica intermediates and QDs;[28] and the sensitive surface of free QDs. In addition, there is no report on the size-dependence of photo- and chemical stability, and the cell uptake of these fluorescent QDs@SiO_2 NPs.

In this study, we designed a new type of SiO_2@CdTe@SiO_2 (SQS) NPs with multi-CdTe embedded in each NP (refer to Fig. 1A). The strategy starts from the synthesis of thiol-capped SiO_2 core. Subsequently, the surface thiol groups can tightly anchor CdTe NCs on the surface of silica nanospheres to reduce their mobility and improve their stability. Further silica coating over SiO_2@CdTe (SQ) NPs leads to the formation of SQS NPs with multi-CdTe NC cores, which show the highest fluorescence QY ever reported (up to 61%). Following this strategy, we firstly prepared a series of highly fluorescent size-tunable SQS NPs by investigating the influence of reaction parameters including silica precursor sources and their feeding amount, water to surfactant ratio, and ammonia concentration. We then studied the size-dependence of the stability, toxicity and cell-uptake of SQS NPs. This research thus addresses the importance of controlling the overall particle size and shell thickness of core–shell silica-QD NPs in order to achieve high stability, high fluorescence quantum yield and the maximum cell-uptake.

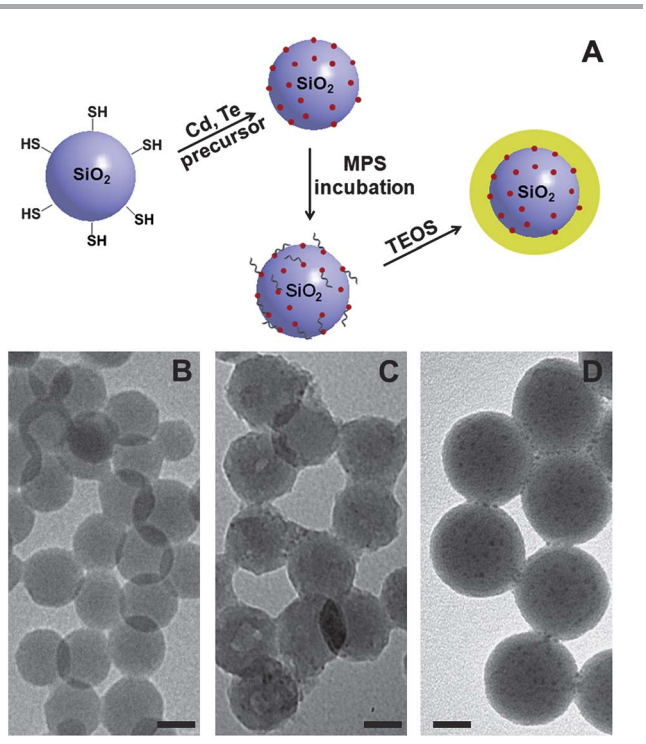

Fig. 1 (A) Scheme of the procedure for preparing SQS NPs and representative TEM images for (B) SiO_2, (C) SQ after MPS incubation, and (D) SQS NPs. Scale bars: 20 nm.

Experimental section

Materials

Cadmium chloride hydrate ($CdCl_2 \cdot 2.5H_2O$), tri-sodium citrate dehydrate (99.3%), sodium tellurite (Na_2TeO_3, 99%), sodium borohydride ($NaBH_4$, 99%), hexyl alcohol (98%), tetraethyl orthosilicate (TEOS, 99.999%), tetramethylorthosilicate (TMOS, 99%), 3-mercaptopropyl-trimethoxysilane (MPS, 99%), thiazolyl blue tetrazolium bromide (MTT), dimethyl sulphoxide (DMSO), and paraformaldehyde (PFA, GR) were purchased from Sigma-Aldrich. Mercaptosuccinic acid (MSA, 99.0%) was ordered from Fluka. Poly-ethylene glycol *tert*-octylphenyl ether (Triton X-100), ammonia solution (25%) and iso-propanol (GR for analysis ACS) were purchased from Merck. Cyclohexane (AR) was ordered from Ajax. RPMI-1640 medium ([+] L-glutamine), ProLong® Gold antifade reagents, and 0.05% trypsin-EDTA were purchased from Invitrogen. Milli-Q water (>18 MΩ) was used in experiments.

Synthesis of silica nanospheres surface-modified with thiol groups

Silica nanospheres were prepared by the reverse microemulsion method according to previous reports.[28] Briefly, 7.5 mL cyclohexane, 1.8 mL *n*-hexanol, and 1.77 mL Triton X-100, 400 μL Milli-Q water, and 240 μL ammonia solution (25 wt%) were added to a flask under stirring, following by 100 μL TEOS or TMOS after stirred for 30 min. The reaction system was then sealed and stirred for three days at room temperature. Subsequently, 10 μL MPS was added and the reaction system was stirred for another 24 h, following by adding 20 mL isopropanol to terminate the reaction. The resultant NP precipitate was washed with isopropanol, ethanol, and water, sequentially. The particles were collected by centrifugation and then redispersed in pure water. The surface thiol groups were determined as described elsewhere.[46,47]

Synthesis of core-satellite SiO_2@CdTe NPs and MPS-incubation

SiO_2@CdTe (SQ) NPs were synthesized *via* a modified procedure according to previous report.[48] Typically, a mixture solution of

silica nanospheres (originated from 1 mL TEOS), cadmium chloride ($CdCl_2$, 0.04 mol L^{-1}, 4 mL) and trisodium citrate dihydrate (400 mg) was diluted to 50 mL in a three-necked flask, and stirred at room temperature for 1 h. Na_2TeO_3 (0.01 mol L^{-1}, 4 mL), mercaptosuccinic acid (100 mg) and sodium borohydride ($NaBH_4$, 50 mg) were then added under vigorous stirring. When the color of the mixture turned to green, the flask was attached to a condenser and refluxed at 100 °C under N_2 flow for 16 h. For MPS-incubation, 50 μL MPS was introduced into the mixture solution at certain time (1–6 h before the completion of the reflux) and continued to reflux. The samples was collected and washed by Milli-Q water for three times. The resultant SQ particles were dispersed in pure water for further synthesis and characterization.

Synthesis of SiO_2@CdTe@SiO_2 NPs

The preparation of SiO_2@CdTe@SiO_2 (SQS) NPs was conducted similarly to the preparation of SiO_2 seeds. Typically, 7.5 mL cyclohexane, 1.8 mL *n*-hexanol, and 1.77 mL Triton X-100, 400 μL as-prepared SQ solutions, and 240 μL ammonia solution (25 wt%) were added to a flask under stirring, followed by introduction of 400 μL TEOS after 30 min. Then, the reaction system was sealed and stirred for three days. Twenty mL isopropanol was added to terminate the reaction, and the resultant NPs were washed with isopropanol, ethanol, and water, sequentially. The final SQS NPs were dispersed in pure water for characterization. When investigating the effect of different parameters on the particle size, TEOS feeding amount is tuned from 50 to 2000 μL; water/surfactant molar ratio was set at 9.3, 13.0, 16.7, and 20.5, respectively; ammonia/TEOS volume ratio was set at 5 : 6, 10 : 6, 15 : 6, and 20 : 6, respectively. When adjusting one parameter, all the others were set the same as that in a typical synthesis described above.

Materials characterization

UV-vis absorption and photoluminescence (PL) intensity spectra were recorded at room temperature with a SpectraMax M5 Multi-mode microplate reader (Molecular devices) in a range of 200 to 800 nm. The transmission electron microscopy (TEM) images of the resultant SiO_2, SQ and SQS NPs were obtained on a JEOL 1010 electron microscope operating at an acceleration voltage of 100 kV. ICP-OES method (Varian Vista Pro ICPOES instrument) was employed to determine the cadmium concentration. Nitrogen adsorption/desorption isotherms were measured at 77 K by using a Micromeritics ASAP Tristar II 3020 system. The samples were degassed at 453 K overnight on a vacuum line. The pore size distribution curves were derived from the adsorption branches of the isotherms using the Barrett–Joyner–Halenda (BJH) method.

Chemical stability test

The SQ and SQS NPs were collected by centrifuge, and then redispersed in solutions with different pH value (5, 7, and 9; the solution pH values were adjusted using hydrochloric acid or sodium hydroxide), respectively. The photoluminescence (PL) of nanoparticle solutions were recorded at certain time intervals, and then compared with that of original solutions by integrating the area of each spectrum.

Photostability test

The photostability of SQS NPs with various shell thicknesses was tested through continuous exposure of their aqueous dispersions to an ultraviolet (UV) irradiation (254 nm) generated by a UV hand lamp (Spectroline, ENF-280C/FE). The PL spectra of the dispersions after exposure for 0–2 h were recorded and the integrated area of the emission peak in each spectrum was calculated and divided by that of the corresponding untreated one.

Cell culture

HEK293 cells (human embryonic kidney cell line) were grown in a monolayer in Roswell Park Memorial Institute (RPMI-1640) Medium supplemented with 10% (v/v) fetal bovine serum (FBS), 2 mM L-glutamine and 100 U mL^{-1} penicillin and streptomycin in a humidified 5% CO_2 atmosphere at 37 °C.

Cell viability assay

Colorimetric 3-(4,5-dimethylthiazol-2-yl)-2,5-diphenyl tetrazolium bromide (MTT) assays were performed to assess the metabolic activity of cells in the presence of NPs. The assay was carried out in quadruplicate in the following manner. HEK293 cells were seeded into a 96-well plate at a density of 2.5×10^4 cells per well in 200 μL of media and grown overnight. The cells were then incubated with SQS NPs at a concentration of 0.2 mg mL^{-1} for 4 h at 37 °C under the humidified atmosphere (5% CO_2) in the dark, after which the medium containing SQS NPs was replaced by fresh culture medium. The cells were then incubated for the desired time (0, 24, and 48 h). Cells were then incubated in media containing 0.5 mg mL^{-1} MTT for 4 h at 37 °C. The medium were removed and 150 μL DMSO was added to each well. The cells were then incubated for 0.5 h at 37 °C. Absorbance was measured at 530 nm by POLARstar OPTIMA Multidetection Microplate Reader (BMG LABTECH). Cell viability, defined as the relative absorbance of each sample compared to that of untreated cells, was calculated and expressed as percentage. The data are presented as the mean ± standard error of the mean (SEM). Two-way ANOVA with Bonferroni post-tests was used to assess statistical significance. $*p < 0.5$, $**p < 0.01$, $***p < 0.001$.

Cellular uptake and intracellular distribution

The cellular uptake and intracellular fate of SQS NPs were examined by flow cytometry and confocal laser scanning microscopy. In the experiment, HEK293 cells were first seeded at 5×10^5 cells per well in 6-well plates (for flow cytometry), or at 2.5×10^5 cells per well in 12-well plates (for CLSM) with one piece of cover glass at the bottom of each well in culture medium overnight. SQS NPs were then added at the concentration of 0.2 mg mL^{-1} for 2 h incubation in 5% CO_2 at 37 °C. For flow cytometry analysis, after the medium was removed, the cells were first digested using 0.25% trypsin, washed with PBS

twice, and finally resuspended in 0.3 mL PBS. Analysis was undertaken on a BD LSR II Flow Cytometer with BD FACSDiva software, version 6.1, using 200 mW of 488 nm laser light as the excitation source. The fluorescence signals of SQS in cells were tracked through a 585/15 bandpass filter. For each sample, 30 000 cells were recorded, and the percentage of SQS-positive cells was calculated. The data are presented as the mean ± SEM. One-way ANOVA with Dunnett's posthoc test was used to assess statistical significance. $*p < 0.5$, $**p < 0.01$, $***p < 0.001$. In confocal microscopy images, the cells were washed with PBS for three times, fixed in 4% PFA for 20 min, and then washed another three times with PBS. The coverslips were then mounted onto Superfrost microscope slides (Menzel-Glaser, Braunschweig, Germany) with ProLong® Gold antifade reagents, and visualized under a laser scanning confocal microscope (Zeiss LSM 510 meta, Germany).

Results and discussion

Particle size and shell thickness control

General morphology of SQS NPs. Fig. 1A displays the procedure for the synthesis of core–shell SQS NPs. Thiol functionalized SiO_2 NPs ($D = 31.5 \pm 2.4$ nm, Fig. 1B) were used as seeds and CdTe nanocrystals were formed *in situ* on their surface. A layer of silica shell was then coated to protect CdTe QDs. During the coating procedure, it is critical to pre-coat SiO_2@CdTe (SQ) NPs with mercaptopropyl-trimethoxysilane (MPS) in order to obtain a final core–shell structure with strong fluorescence. Differently from our previous report in which MPS incubation was carried out at room temperature after synthesis of SQ NPs,[47] we directly added MPS into the reaction mixture under refluxing conditions before the completion of SQ preparation. The SQ samples were collected at different time points after addition of MPS and their fluorescence spectra were measured after purification. The data (ESI Fig. S1A†) demonstrated that MPS incubation could improve the fluorescence intensity of CdTe QDs and the optimal incubation time was 3–4 h, when the strongest fluorescence (QY = ~75%) was obtained. In addition, the MPS feeding amount is also found to be critical. The optimal MPS amount can assist TEOS monomers to deposit on the SQ surface and results in regular spherical NPs. However, excessive MPS led to a rough surface and failure of subsequent silica coating (Fig. S1B†). The typical TEM images of SQ and SQS NPs obtained from the optimal MPS are shown in Fig. 1(C) and (D), and their average sizes are 41.3 ± 2.7 nm, and 54.2 ± 2.2 nm, respectively.

It should be noted that some SiO_2 NPs were partially damaged during preparation of SQ NPs. These looked like porous NPs. To further confirm their structures, nitrogen adsorption isotherms of SiO_2, SQ and SQS were performed and the pore size distributions were calculated using the BJH method. In Fig. S2† that shows the adsorption–desorption plot of SQ NPs, the capillary condensation step occurred only at high relative pressure ($P/P_0 > 0.9$) due to the interparticle porosity formed by the aggregation of nanospheres.[49,50] Additional evidence leading to the same conclusion came from the pore-size distribution curves of SiO_2, SQ, and SQS (inset of Fig. S2†), where the peaks of three curves ranged from 40 to 80 nm, demonstrating the non-porous structures of all three NPs. In order to determine the reason for the particle damage, we carried out a control experiment in which only thiol-capped SiO_2 NPs and $NaBH_4$ were mixed and the mixture solution was refluxed under the same conditions applied in the synthesis of SQ NPs. Similarly damaged SiO_2 NPs were found in this sample (Fig. S3†). It is thus believed that H_2 bubbles released from $NaBH_4$ are responsible for the damage of NPs. The damaged NPs are slightly aggregated in comparison with undamaged ones.

Particle size control-adjusting the shell thickness. The reverse microemulsion approach has been progressively developed to synthesize pure silica NPs. A number of studies have demonstrated that the particle size can be controlled by adjusting various parameters.[43,51] The microemulsion system consists of water, oil, (co)-surfactant, silica precursor and ammonia solution, and the reproducibility of this approach is a big issue due to its complexity. Here we investigated the influence of these factors on the overall particle size and silica shell thickness in the silica coating process. Three main factors were selected for the investigation, including TEOS feeding amount, [H_2O]/[Triton X-100] ratio, and ammonia/TEOS ratio. Fig. 2 presents the dependence of SQS particle size on TEOS feeding amount. The data show that the particle size can be tuned from 48 to 76 nm by adjusting TEOS feeding amount from 50 to 2000 μL (see Table 1 for details). Assuming the SQ size was 41.3 nm, the silica shell thickness varied from 4 to 18 nm. The TEM images and particle size distributions of these samples can be found in Fig. S4–12.† When the TEOS amount was less than 200 μL, the resultant NPs had a wide size distribution and the standard deviation was larger than 4 nm, due to the presence of incompletely wrapped NPs (Fig. S5–7†). One typical sample was prepared using 100 μL TEOS, which showed two peaks in its size distribution histogram (Fig. S6†). One peak located at around 42 nm corresponds to SQ NPs, the other one at 58 nm represents SQS NPs. When more than 300 μL TEOS was fed (Fig. S8–12†), monodispersed core–shell NPs with a narrow size distribution and an increased shell thickness were successfully synthesized.

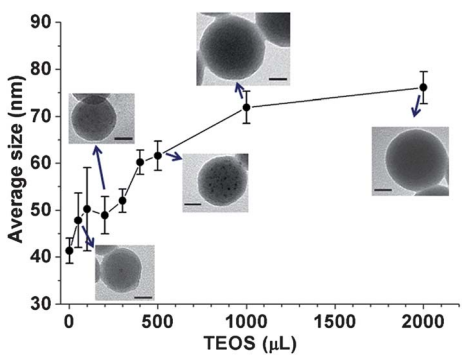

Fig. 2 Shell thickness and overall particle size control by adjusting the feeding amount of TEOS. The insets are TEM images of selective SQS NPs from samples with TEOS feeding amount of 50, 200, 500, 1000, and 2000 μL, respectively. Scale bars in all insets equal to 20 nm.

Table 1 Overall particle sizes and corresponding silica shell thicknesses of SQ and SQS NPs prepared in this research

Silica core precursor	NPs' name	Overall particle size (nm)	Silica shell thickness (nm)
TEOS	SQ41	41.3 ± 2.7	0
	SQS48	47.8 ± 5.8	3.3
	SQS50	50.2 ± 8.9	4.5
	SQS52	52.0 ± 2.5	5.4
	SQS62	61.6 ± 3.1	10.2
	SQS72	71.9 ± 3.4	15.3
	SQS76	76.1 ± 3.4	17.4
TMOS[a]	SQ19	18.9 ± 1.8	0
	SQS39	39.2 ± 2.6	10.2

[a] The synthesis and features of the NPs will be described in detail in the following context.

The molar ratio of $[H_2O]/[\text{Triton X-100}]$ (R_M) was found to be another factor that could affect the silica shell thickness and the final particle size. As shown in Fig. 3A, at R_M of 9.3 (TEOS of 400 μL, Triton X-100 of 1.77 mL), the final average particle size of SQS was around 60 nm. With the increase of R_M, the average particle size decreased, accompanied with the broadening of the particle size distribution. When R_M reached 20.5, the particle size decreased to 40 nm, indicating that almost no silica shell was deposited on the particle surface. A typical TEM image of this sample is shown in Fig. S13,† and no coating shell could be observed. Instead of being embedded inside, CdTe QDs aggregated on the surface of SiO_2 NPs. Simultaneously, more and more QD-free silica NPs were observed in TEM images with the increase of R_M. This is quite different from the previous study, in which the particle size was reported to be in direct proportion to R_M.[44] A possible reason might be the increase of micelle volume in the microemulsion system. The increase of micelle volume results in a decrease of SQ concentration in water phase, or alternatively, less SQ NPs in each micelle. It is known that the hydrolysis of TEOS occurs at the interface of reverse micelles in the microemulsion system. The hydrolyzed TEOS monomers are then condensed into small nuclei which normally act as seeds for the growth of NPs. In the current case, the hydrolyzed TEOS monomers either diffuse to the surface of SQ or form new nuclei for the growth of silica NPs. The decreased number of SQ NPs in each micelle suggests a longer path and time for hydrolyzed TEOS monomers to diffuse to SQ surface and thus increased the chance for the formation of new nuclei. Newly formed nuclei compete with SQ NPs in consuming TEOS monomers, and thus result in QD-free silica NPs. The evidence could be found in the case of $R_M = 20.5$, where uncoated SQ and a large quantity of QD-free silica NPs were observed (Fig. S13†).

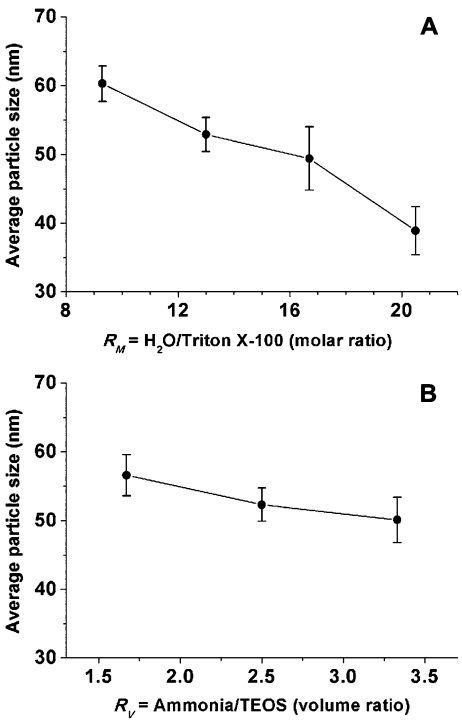

Fig. 3 The effect of (A) water phase to surfactant molar ratio and (B) ammonia to TEOS volume ratio on the particle size of SQS NPs.

Ammonia solution is used to catalyze the hydrolysis of TEOS, thus significantly influencing particle size and morphology. To evaluate the effect of ammonia concentration, we fixed R_M at 9.3 and TEOS amount at 400 μL. TEM images (Fig. S14†) reveal that at a low ammonia concentration (*i.e.* ammonia/TEOS volume ratio $R_V = 0.8$, Fig. S14A†), large aggregated particles with only a few individual NPs were obtained. With R_V increasing from 0.8 to 1.7, monodispersed NPs were formed (Fig. S14B†). Further increase of R_V from 1.7 to 2.5 led to a slight decrease in the particle size, and an improved surface smoothness (Fig. S14C†). Some small amorphous granules were found at the highest ammonia/TEOS ratio (*i.e.* $R_V = 3.3$, Fig. S14D†). The particle size–R_V curve is shown in Fig. 3B. As R_V increased from 1.7 to 3.3, the average particle size decreased from 56.6 to 50.1 nm. According to the previous study, changing ammonia volume may affect the hydrolysis and condensation reactions of TEOS and the tendency of siloxane bond breaking in highly alkaline solution.[51] At a relatively low ammonia concentration ($R_V = 0.8$), the hydrolysis of TEOS is so slow that TEOS monomers are not enough to evenly deposit on the SQ surface and prefer to deposit onto the surface with SiO_2 exposure. As a result, some NPs grow ever larger while others cease to grow or grow slowly. With more ammonia added, the fast hydrolysis of TEOS allows even deposition of TEOS monomers on the SQ NPs surface. All the NPs can grow simultaneously to form monodispersed NPs with a narrow size distribution. However, when too much ammonia solution is used (*i.e.* $R_V = 3.3$), too fast TEOS hydrolysis would result in the formation of some small QD-free NPs. In brief, the above observations suggest that controlling the amount of TEOS could be the best way to tune the SQS particle size and shell thickness.

Particle size control-tuning the core size. The minimal average particle size of wholly and evenly wrapped SQS NPs in our samples was 52 nm, with silica shell of about 6 nm. In order to prepare core–shell NPs smaller than 50 nm, we prepared smaller SiO_2 cores by using TMOS as the silica precursor. TMOS is also commonly used to synthesize silica NPs in many studies

due to its faster hydrolysis than TEOS. On one hand, the faster hydrolysis of TMOS leads to a burst of nucleation and formation of small particles. We successfully obtained SiO_2 NPs with an average diameter of 16.7 ± 1.2 nm, much smaller than that obtained from TEOS (D = 31.5 ± 2.4 nm). On the other hand, the fast hydrolysis of TMOS makes it unsuitable for silica coating, because the rapidly hydrolyzed TMOS tends to form nuclei rather than to deposit on the SQ surface. Therefore, we continued to use TEOS as precursor for the silica coating. Following the same procedure shown in Fig. 1A, we did obtain smaller SQS NPs (39.2 ± 2.6 nm) from 18.9 nm SQ cores. Fig. 4 shows the typical TEM images of SiO_2 and SQS NPs obtained in the preparation. In SQ NPs (not shown), damage and aggregation of silica cores similar to that observed in Fig. S3† were also found. However, after silica coating (Fig. 4B), the interface between the core and shell could be identified clearly, and the silica shell was calculated to be ~10 nm (Table 1), which is thick enough for effective protection for wrapped CdTe QDs, as discussed in the following section.

The effects of SQS particle size and shell thickness on their properties

Silica shell protection to QDs. Previously we reported the highest fluorescence efficiency (QY ~ 61%) for SQS NPs.[47] With an improved MPS incubation procedure, we thus obtained a series of such highly fluorescent SQS NPs with controllable morphology. The representative absorption and fluorescence spectra of SQ were shown in Fig. S15(A),† and the fluorescence spectra of SQ after MPS-incubation and corresponding SQS NPs can be found in Fig. S15(B),† showing limited loss (~15%) in fluorescence after silica coating. This is better than the previous reports in which more than 40% fluorescence was lost during silica coating.[45]

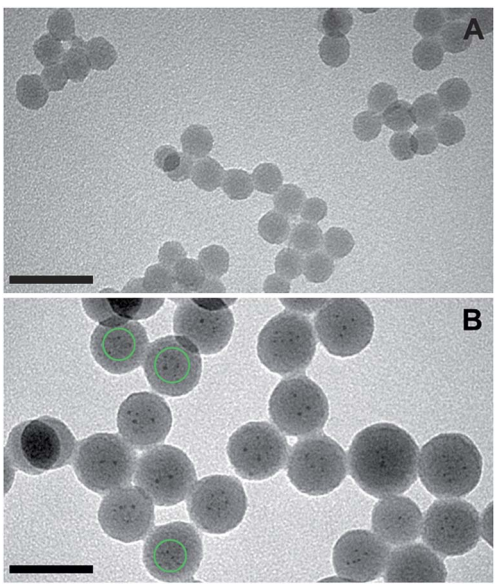

Fig. 4 TEM images of (A) SiO_2 and (B) corresponding SQS NPs with TMOS as silica source in the synthesis of silica core. SQ cores were circled in dash lines in (B). Scale bars: 50 nm.

The external silica shell is expected to provide protection to the internal CdTe QDs. Therefore, we tested the chemical and photo-stability of SQS NPs with different shell thickness, together with SQ NPs. The fluorescence retention of SQS NP solutions with different pH is shown in Fig. S16.† Both SQ NPs and SQS NPs were found to be stable in a pH range of 6–9. At pH = 5, the fluorescence of SQ NPs started to decrease from 6 h and dropped by nearly 20% after 24 h (Fig. S16A†). Similar fluorescence quenching was also found in SQS48 (silica shell of 3 nm) (Fig. S16B†). With the shell increasing to above 5 nm, the fluorescence of the embedded QDs was no longer quenched. Fig. S16C and D† show the time-dependence of fluorescence observed in SQS52 and SQS62 NPs. The fluorescence was maintained and there was no decrease in fluorescence intensity. The dependence of chemical stability on the shell thickness demonstrates that it is necessary to coat SQ NPs with at least a 5 nm silica shell in order to effectively prevent fluorescence quenching in a pH window of 5–9.

Similar trends have also been found in photo-oxidation experiments. Fig. S17† presents the fluorescence retention of SQS NPs after exposure to UV light, in comparison with that of mercaptosuccinic acid (MSA)-capped CdTe QDs and SQ NPs.

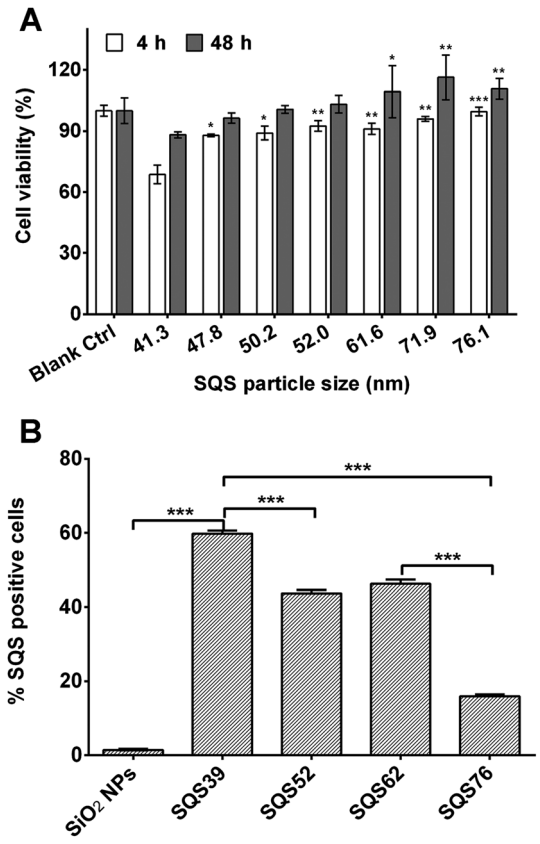

Fig. 5 (A) HEK293 cell cytotoxicity of SQ41 and SQS NPs with various particle size. All the values are the means ± standard error of the mean (SEM) from four independent experiments. At each time point, the cell viability of each NP was compared against that of SQ41 NPs. (B) SQS NP uptake by HEK293 cells. Cells were exposed to NPs (200 μg mL^{-1}, 2 h). Uptake values are the means ± SEM of the percentage of SQS positive cells from three independent experiments. *p < 0.5, **p < 0.01, ***p < 0.001.

The fluorescence of MSA-capped CdTe QDs decreased by 25% after only 20 min of continuous UV light ($\lambda = 254$ nm) irradiation, and became stable up to 120 min, indicating slight fluctuations in fluorescence intensity. For SQ and SQS48 NPs, 15% of the fluorescence was lost after 20 min continuous UV irradiation. In contrast, SQS52 and SQS62 NPs maintained nearly 100% fluorescence after 120 min UV irradiation. These results demonstrate that thicker silica shell protected QD well than thinner shell.

Effect of particle size on cell viability and cellular uptake efficiency. The toxicity of core–shell SQS NPs was evaluated by the MTT assay. In the experiments, SQ41 and SQS NPs of different sizes (47.8–76.1 nm) were incubated with HEK293 cells for 4 h, after which the medium was replaced with the fresh medium. Cell viability was tested immediately and after further 48 h incubation. At each time point, the cell viability of blank control was set as "100%", and the absorbance value of each sample was compared to that of the blank control (*i.e.* untreated cells), and expressed as percentage. As shown in Fig. 5A, cell viability was reduced to 69% after exposure to the SQ41 NPs for 4 h. In contrast, exposure to SQS52 NPs resulted in 10–15% decrease in viability after incubation for 4 h. Moreover, SQS52, 62, 72, and 76 NPs all resulted in more than 90% cell viability. In addition, in cases of SQS62, 72, and 76 NPs, increased cell viability was observed after 48 h culture in the absence of NPs. The MTT results demonstrate that silica shell can effectively decrease the toxicity inherently caused by QDs, and a thicker shell (>5 nm) can provide better protection.

As mentioned in the introduction, the nanoparticle size can significantly influence their biological behavior, including cellular internalization.[30,31] We chose four SQS NPs (SQS39, 52, 62, and 76) to investigate their uptake efficiency in HEK293 cells using flow cytometry. Untreated cells were used as the blank control, and 40 nm pure silica NPs without QDs were selected as the negative control. For each measurement, 30 000 cells were counted. The percentage of SQS-positive cells (using blank control as background) is displayed in Fig. 5B. The highest cellular uptake (~60%) occurred for SQS39 NPs, whereas approximately 50% of cells internalized the SQS52 and SQS62 NPs. In the case of SQS76, less than 20% cells were positive.

These results demonstrate a strong size-dependent cellular uptake of SQS NPs, indicating that a SQS particle size of less than 70 nm is optimum for efficient uptake by HEK293 cells.

We next examined the intracellular distribution of SQS NPs using a confocal laser scanning microscope (CLSM). After incubation with NPs for 2 h, HEK293 cells were fixed and stained by 4′-6-diamidino-2-phenylindole (DAPI), and then observed under CLSM. Fig. 6 presents the intracellular distribution after uptake of SQS NPs. SQS39 and SQS52 NPs were seen to distribute in both the cytoplasm and nucleus, where the red fluorescence signal in the cytoplasm was stronger than in the nucleus. However, larger NPs (SQS62) were located mainly in

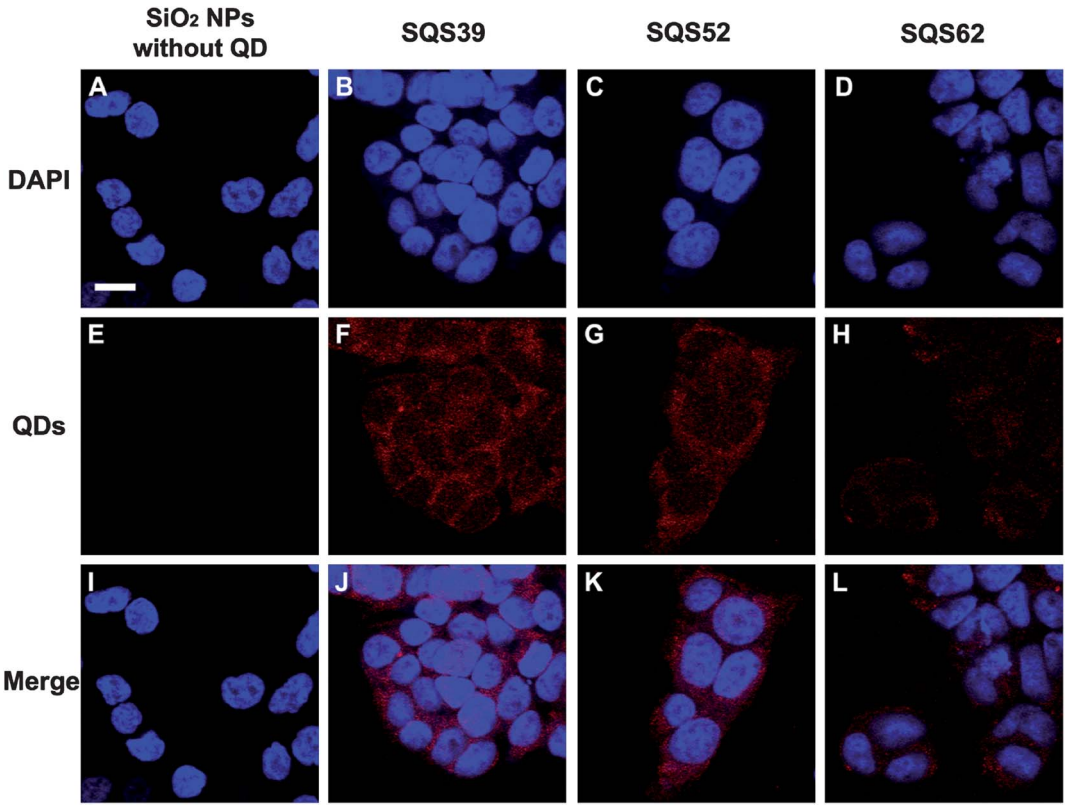

Fig. 6 CLSM images of HEK293 cells treated with (A, E and I) SiO_2 NPs without QDs, (B, F and J) SQS39, (C, G and K) SQS52, and (D, H and L) SQS62. (A–D) DAPI (blue), (E–H) QDs (red), and (I–L) merged images. Scale bar: 10 μm.

the cytoplasm. Fig. S18† gives the 3D structure created from Z-stack images originated from Fig. 6J, clearly showing SQS39 NPs located within the nucleus.

The cellular uptake results demonstrate that our SQS were distributed more in cytoplasm than in nucleus. The distribution in nucleus decreased with the increase in particle size. It should be noted that the exact entry mechanism of NPs into the cell nucleus is unclear. It appears to be strongly dependent on the particle size, shape and/or surface properties. An early report suggests that only molecules (particles) smaller than 9 nm can enter the nucleus by diffusion because the patent radius of nuclear pores is about 45 Å.[52] However, Dworetzky *et al.* found that larger molecules up to 39 nm with BSA-coating can enter the nucleus by active transport *via* the nuclear pore complex.[53] Several other studies support the contention that NPs larger than 50 nm can enter the nucleus when they are additionally coupled to a nuclear localization sequence.[54–57] Chen *et al.* showed that 70 nm FITC–SiO_2 NPs could enter the nuclei of human epithelial Hep-2 cells, but induced aberrant clusters of topoisomerase I (topo I) and protein aggregation in the nucleoplasm.[58] Although the intranuclear protein aggregates have no significant effect on proteasomal activity and cell viability, they will inhibit replication, transcription, and cell proliferation. Herein we observed similar nuclear uptake of SQS NPs (39 and 52 nm) by HEK293 cells. Our MTT assay shows that SQS NPs had little effect on cell viability for 48 h. Although more evidence is needed to confirm whether SQS NPs affect cell proliferation, current results have already demonstrated that SQS NPs exhibit remarkably improved biocompatibility compared to unmodified CdTe QDs and SQ NPs, based on the high fluorescence retention.

Conclusions

In summary, we have successfully synthesized a series of size tunable core–shell SQS NPs. By adjusting both silica core size and shell thickness, the overall particle size can be controlled in the range of 39–76 nm. The shell thickness can be tuned by controlling TEOS feeding amount, water phase concentration, and ammonia concentration. Silica coating has significantly improved the chemical stability, photostability and biocompatibility of inside CdTe QDs. MTT assay, flow cytometry analysis and CLSM images show strong size dependence of cytotoxicity, cellular uptake, and intracellular distribution. The lower toxicity, higher stability and strong fluorescence of our core–shell SQS NPs make them robust probes for bioimaging.

Acknowledgements

This work has been financially supported by the Australian Research Council through a Discovery Project Grant (DP0879769). Y.Z. thanks the UQ International Research Tuition Awards. Z.L. gratefully acknowledges the support from Queensland Smart Futures Fellowship, and University of Wollongong AIIM Collaborative Research Grant. H.M.C. gratefully acknowledges support from the Queensland Smart Futures Fellowship Scheme. Z.P. Xu. gratefully acknowledges the ARC Australian Research Fellow (ARF) Scheme.

Notes and references

1 B. Dubertret, P. Skourides, D. J. Norris, V. Noireaux, A. H. Brivanlou and A. Libchaber, *Science*, 2002, **298**, 1759–1762.
2 M. K. So, C. J. Xu, A. M. Loening, S. S. Gambhir and J. H. Rao, *Nat. Biotechnol.*, 2006, **24**, 339–343.
3 L. M. Maestro, E. M. Rodriguez, F. S. Rodriguez, M. C. I. la Cruz, A. Juarranz, R. Naccache, F. Vetrone, D. Jaque, J. A. Capobianco and J. G. Sole, *Nano Lett.*, 2010, **10**, 5109–5115.
4 W. W. Wang, D. Cheng, F. M. Gong, X. M. Miao and X. T. Shuai, *Adv. Mater.*, 2012, **24**, 115–120.
5 U. Resch-Genger, M. Grabolle, S. Cavaliere-Jaricot, R. Nitschke and T. Nann, *Nat. Methods*, 2008, **5**, 763–775.
6 Y. F. Loginova, S. V. Dezhurov, V. V. Zherdeva, N. I. Kazachkina, M. S. Wakstein and A. P. Savitsky, *Biochem. Biophys. Res. Commun.*, 2012, **419**, 54–59.
7 L. Ye, K. T. Yong, L. W. Liu, I. Roy, R. Hu, J. Zhu, H. X. Cai, W. C. Law, J. W. Liu, K. Wang, J. Liu, Y. Q. Liu, Y. Z. Hu, X. H. Zhang, M. T. Swihart and P. N. Prasad, *Nat. Nanotechnol.*, 2012, **7**, 453–458.
8 W. Zhang, K. F. Lin, Y. N. Miao, Q. X. Dong, C. J. Huang, H. L. Wang, M. J. Guo and X. H. Cui, *J. Hazard. Mater.*, 2012, **213**, 413–420.
9 Y. Zhu, Z. Li, M. Chen, H. M. Cooper, G. Q. Lu and Z. P. Xu, *J. Colloid Interface Sci.*, 2013, **390**, 3–10.
10 L. Li, T. J. Daou, I. Texier, T. K. C. Tran, Q. L. Nguyen and P. Reiss, *Chem. Mater.*, 2009, **21**, 2422–2429.
11 J. Park, J. Nam, N. Won, H. Jin, S. Jung, S. Jung, S. H. Cho and S. Kim, *Adv. Funct. Mater.*, 2011, **21**, 1558–1566.
12 X. H. Gao, Y. Y. Cui, R. M. Levenson, L. W. K. Chung and S. M. Nie, *Nat. Biotechnol.*, 2004, **22**, 969–976.
13 V. L. Colvin, W. W. Yu, E. Chang, J. C. Falkner, J. Y. Zhang, A. M. Al-Somali, C. M. Sayes, J. Johns and R. Drezek, *J. Am. Chem. Soc.*, 2007, **129**, 2871–2879.
14 W. B. Cai and X. Y. Chen, *Nat. Protoc.*, 2008, **3**, 89–96.
15 H. W. Duan and S. M. Nie, *J. Am. Chem. Soc.*, 2007, **129**, 3333–3338.
16 J. B. Liu, X. H. Yang, K. M. Wang, Q. Wang, H. N. Ji, C. L. Wu, J. Li, X. X. He, J. L. Tang and J. Huang, *J. Mater. Chem.*, 2012, **22**, 495–501.
17 W. T. Al-Jamal, K. T. Al-Jamal, P. H. Bomans, P. M. Frederik and K. Kostarelos, *Small*, 2008, **4**, 1406–1415.
18 C. J. Wen, L. W. Zhang, S. A. Al-Suwayeh, T. C. Yen and J. Y. Fang, *Int. J. Nanomed.*, 2012, **7**, 1599–1611.
19 K. C. Weng, C. O. Noble, B. Papahadjopoulos-Sternberg, F. F. Chen, D. C. Drummond, D. B. Kirpotin, D. H. Wang, Y. K. Hom, B. Hann and J. W. Park, *Nano Lett.*, 2008, **8**, 2851–2857.
20 A. M. Derfus, W. C. W. Chan and S. N. Bhatia, *Nano Lett.*, 2004, **4**, 11–18.

21 C. Kirchner, T. Liedl, S. Kudera, T. Pellegrino, A. M. Javier, H. E. Gaub, S. Stolzle, N. Fertig and W. J. Parak, *Nano Lett.*, 2005, **5**, 331–338.
22 M. Bruchez, M. Moronne, P. Gin, S. Weiss and A. P. Alivisatos, *Science*, 1998, **281**, 2013–2016.
23 D. V. Szabo and D. Vollath, *Adv. Mater.*, 1999, **11**, 1313–1316.
24 A. L. Rogach, D. Nagesha, J. W. Ostrander, M. Giersig and N. A. Kotov, *Chem. Mater.*, 2000, **12**, 2676–2685.
25 V. Salgueiriño-Maceira, M. A. Correa-Duarte, M. Spasova, L. M. Liz-Marzan and M. Farle, *Adv. Funct. Mater.*, 2006, **16**, 509–514.
26 J. E. Fuller, G. T. Zugates, L. S. Ferreira, H. S. Ow, N. N. Nguyen, U. B. Wiesner and R. S. Langer, *Biomaterials*, 2008, **29**, 1526–1532.
27 H. S. Yang, P. H. Holloway and S. Santra, *J. Chem. Phys.*, 2004, **121**, 7421–7426.
28 Y. H. Yang and M. Y. Gao, *Adv. Mater.*, 2005, **17**, 2354–2357.
29 P. Yang, M. Ando and N. Murase, *J. Colloid Interface Sci.*, 2011, **354**, 455–460.
30 G. Applerot, A. Lipovsky, R. Dror, N. Perkas, Y. Nitzan, R. Lubart and A. Gedanken, *Adv. Funct. Mater.*, 2009, **19**, 842–852.
31 E. Oh, J. B. Delehanty, K. E. Sapsford, K. Susumu, R. Goswami, J. B. Blanco-Canosa, P. E. Dawson, J. Granek, M. Shoff, Q. Zhang, P. L. Goering, A. Huston and I. L. Medintz, *ACS Nano*, 2011, **5**, 6434–6448.
32 S. D. Perrault and W. C. W. Chan, *Proc. Natl. Acad. Sci. U. S. A.*, 2010, **107**, 11194–11199.
33 C. H. J. Choi, J. E. Zuckerman, P. Webster and M. E. Davis, *Proc. Natl. Acad. Sci. U. S. A.*, 2011, **108**, 6656–6661.
34 P. Decuzzi, B. Godin, T. Tanaka, S. Y. Lee, C. Chiappini, X. Liu and M. Ferrari, *J. Controlled Release*, 2010, **141**, 320–327.
35 H. S. Choi, W. Liu, P. Misra, E. Tanaka, J. P. Zimmer, B. I. Ipe, M. G. Bawendi and J. V. Frangioni, *Nat. Biotechnol.*, 2007, **25**, 1165–1170.
36 B. D. Chithrani and W. C. W. Chan, *Nano Lett.*, 2007, **7**, 1542–1550.
37 F. Lu, S. H. Wu, Y. Hung and C. Y. Mou, *Small*, 2009, **5**, 1408–1413.
38 H. Jin, D. A. Heller, R. Sharma and M. S. Strano, *ACS Nano*, 2009, **3**, 149–158.
39 W. Jiang, B. Y. S. Kim, J. T. Rutka and W. C. W. Chan, *Nat. Nanotechnol.*, 2008, **3**, 145–150.
40 H. Wang, S. T. Wang, H. Su, K. J. Chen, A. L. Armijo, W. Y. Lin, Y. J. Wang, J. Sun, K. Kamei, J. Czernin, C. G. Radu and H. R. Tseng, *Angew. Chem., Int. Ed.*, 2009, **48**, 4344–4348.
41 S. D. Perrault, C. Walkey, T. Jennings, H. C. Fischer and W. C. W. Chan, *Nano Lett.*, 2009, **9**, 1909–1915.
42 Y. H. Yang, L. H. Jing, X. L. Yu, D. D. Yan and M. Y. Gao, *Chem. Mater.*, 2007, **19**, 4123–4128.
43 C. L. Chang and H. S. Fogler, *Langmuir*, 1997, **13**, 3295–3307.
44 L. Yao, G. Y. Xu, W. L. Dou and Y. Bai, *Colloids Surf., A*, 2008, **316**, 8–14.
45 L. H. Jing, C. H. Yang, R. R. Qiao, M. Niu, M. H. Du, D. Y. Wang and M. Y. Gao, *Chem. Mater.*, 2010, **22**, 420–427.
46 Z. Li, B. Tan, M. Allix, A. I. Cooper and M. J. Rosseinsky, *Small*, 2008, **4**, 231–239.
47 Y. Zhu, Z. Li, M. Chen, H. M. Cooper, G. Q. Lu and Z. P. Xu, *Chem. Mater.*, 2012, **24**, 421–423.
48 H. F. Bao, E. K. Wang and S. J. Dong, *Small*, 2006, **2**, 476–480.
49 M. H. Yu, L. Zhou, J. Zhang, P. Yuan, P. Thorn, W. Y. Gu and C. Z. Yu, *J. Colloid Interface Sci.*, 2012, **376**, 67–75.
50 K. Suzuki, K. Ikari and H. Imai, *J. Am. Chem. Soc.*, 2004, **126**, 462–463.
51 F. J. Arriagada and K. Osseo-Asare, *J. Colloid Interface Sci.*, 1999, **211**, 210–220.
52 P. L. Paine, L. C. Moore and S. B. Horowitz, *Nature*, 1975, **254**, 109–114.
53 S. I. Dworetzky, R. E. Lanford and C. M. Feldherr, *J. Cell Biol.*, 1988, **107**, 1279–1287.
54 I. Nabiev, S. Mitchell, A. Davies, Y. Williams, D. Kelleher, R. Moore, Y. K. Gun'ko, S. Byrne, Y. P. Rakovich, J. F. Donegan, A. Sukhanova, J. Conroy, D. Cottell, N. Gaponik, A. Rogach and Y. Volkov, *Nano Lett.*, 2007, **7**, 3452–3461.
55 P. Nativo, I. A. Prior and M. Brust, *ACS Nano*, 2008, **2**, 1639–1644.
56 S. Singh, A. Kumar, A. Karakoti, S. Seal and W. T. Self, *Mol. BioSyst.*, 2010, **6**, 1813–1820.
57 M. Al-Rawi, S. Diabate and C. Weiss, *Arch. Toxicol.*, 2011, **85**, 813–826.
58 M. Chen and A. von Mikecz, *Exp. Cell Res.*, 2005, **305**, 51–62.